Error analysis for CGH optical testing

Yu-Chun Chang*[a] and James Burge[b]

[a]Hewlett-Packard Company, San Jose, CA 95135

[b]Optical Sciences Center, University of Arizona, Tucson, AZ 85721

ABSTRACT

Computer generated holograms are widely used in optical testing and metrology. The primary role of the CGHs is to generate reference wavefront with any desired shape. Optical or electron-beam writers are commonly used for CGH fabrication. Limitations from the hologram fabrication processes cause errors in the reproduced wavefront. Errors in duty-cycle and etching depth have direct impact on both the amplitude and phase functions of the reproduced wavefront. A study using scalar diffraction model to simulate CGH fabrication errors and their effects on wavefront amplitude and phase functions are presented. Experimental analysis confirms the theoretical model. An example is given at the end to demonstrate one of the many applications of the wavefront sensitivity functions in CGH error budgeting for optical metrology.

Keywords: *Optical testing, Interferometry, Computer-generated holograms, errors analysis.*

1. INTRODUCTION

Computer-generated holograms (CGHs) are diffractive optical elements synthesized using the aid of computers. They are capable of producing optical wavefronts with any desired shape. This high degree of flexibility in generating complex wavefronts has made CGHs extremely useful. In the field of optical testing and metrology, CGHs are commonly used in optical interferometric system for measuring aspheric optics. The precision of CGHs affects the accuracy and validation of measured results. Errors and uncertainties during the CGH fabrication processes, however, result in errors in the diffraction wavefronts created by the finished hologram. When applying the finished hologram in optical testing, precision of the measurement results will be affected consequently.

This paper addresses the effects of CGH fabrication errors on the accuracy of interferometric measurements. Possible sources of error in CGH fabrication such as substrate figure errors, pattern distortion, duty-cycle and etching depth variations are investigated. The dependencies of the diffracted wavefront phase on these fabrication uncertainties are examined. These results are used to analyze the performance of a phase hologram in optical testing.

2. SOURCE OF ERRORS DUE TO CGH FABRICATION LIMITATION

A computer-generated hologram for optical testing usually consists of patterns of curved lines drawn onto or etched into a substrate material. The patterns act as diffraction gratings that use variations in the spacing to control the distribution of diffracted light. Errors in both the recorded grating pattern and the shape of the substrate contribute to the errors in the reproduced diffraction wavefront.

Traditional method for fabricating computer-generated holograms is done through automated plotting and photographic reduction.[1] This fabrication process was time consuming and accuracy of this fabrication process was limited by the resolution of the plotter and errors associated with the photo-reduction process. Nowadays, state of the art laser beam and electron-beam lithography technology allows CGHs to be directly written at their finished size, which eliminate the photo-reduction process. Micro-lithography also allows the hologram to be generated at a much higher accuracy than the

Part of the SPIE Conference on Optical Manufacturing and Testing III
Denver, Colorado • July 1999
SPIE Vol. 3782 • 0277-786X/99/$10.00

conventional photo-reproduction process. This fabrication method has made it possible to manufacture holograms with high precision and finesse.

CGH fabrication errors may be classified into two basic types: substrate figure errors and pattern errors. Pattern errors may further be classified as fringe position errors, fringe duty-cycle errors and fringe etching depth errors. These CGH fabrication errors will be discussed in detail in the following sections.

3. ERROR ANALYSIS FOR CGHS

The simplest form of a hologram is a linear diffraction grating, where the spatial frequency of the grating pattern is constant over the entire hologram. A computer-generated hologram with variable fringe spacing may be viewed as a collection of linear gratings with variable spatial frequency. By controlling the spatial frequencies of these linear gratings across the CGH, incident light can be deflected into any desired form.[2] The performance of a CGH may, therefore, be directly related to the diffraction characteristics of a linear grating. Linear gratings are often used for studies on CGH properties in order to avoid mathematical difficulties in modeling complex hologram fringe patterns. To reduce the degree of complexity of our study, linear gratings are also chosen as the model for our work.

3.1. Binary Linear Grating Model

The linear grating model used in our studies is assumed to have binary amplitude and phase distributions. A binary linear grating has a surface relief profile that may be described as an infinite train of rectangular pulses with a uniform width. The wavelength of the incident light is assumed to be much smaller than to the grating period (S), so the scalar diffraction approximations can be applied.[3] For a planar wavefront at normal incidence, the output wavefront immediately past the grating, either reflected or transmitted, can be expressed as a simple product of the incident wavefront function and the grating surface profile function. The output wavefront function can be written as:

$$u(x) = A_0 + (A_1 e^{i\phi} - A_0)\,\mathrm{rect}\left(\frac{x}{b}\right) * \frac{1}{S}\,\mathrm{comb}\left(\frac{x}{S}\right) \tag{1}$$

where A_0 and A_1 correspond to the amplitude values of the output wavefront from the peaks and valleys of the grating, respectively. The values of A_0 and A_1 are determined from the amplitude functions of the reflectance or the transmittance coefficients at the grating interface using Fresnel equations.[4] The phase function, ϕ, represents the phase difference between rays from the peaks and rays from the valleys of the grating structure. The form of the output wavefront function (Fig. 1) resembles the shape of the grating profile.

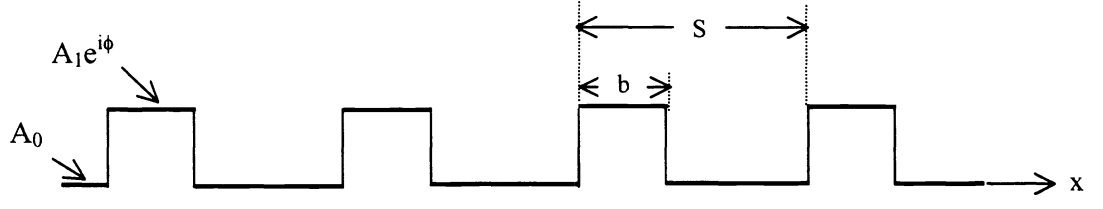

Fig. 1 Output complex wavefront function at the diffraction grating.

In this study, we are mostly interested in the behaviors of the diffraction wavefront in the far-field regime. The far-field diffraction wavefront is related to the original wavefront via a simply Fourier transform relationship based on the Fraunhofer diffraction theory. Hence, the far-field wavefront function of a normal incident plane wavefront upon the grating described in Eq. (1) is:

$$U(\xi) = \Im\{u(x)\} \tag{2}$$

$$\begin{aligned} U(\xi) &= A_0\delta(\xi) + \left(A_1 e^{i\phi} - A_0\right)\cdot b\cdot \mathrm{sinc}(b\xi)\cdot \mathrm{comb}(S\xi) \\ &= A_0\delta(\xi) + \left(A_1 e^{i\phi} - A_0\right)\cdot D\cdot S\cdot \mathrm{sinc}(DS\xi)\cdot \mathrm{comb}(S\xi) \end{aligned} \tag{3}$$

$$= \begin{cases} \{ A_0 + [A_1 \cos(\phi) - A_0] \cdot D \} + i\{ A_1 \sin(\phi) \cdot D \}; & m = 0 \\ \{ [A_1 \cos(\phi) - A_0] \cdot D \cdot \sin c(mD) \} + i\{ A_1 \sin(\phi) \cdot D \cdot \sin c(mD) \}; & m = \pm 1, \pm 2, \ldots \end{cases}$$

where $\xi = \frac{x'}{\lambda z}$ and the duty-cycle of the linear grating is $D = \frac{b}{S}$.

Eq. (3) shows that the diffraction wavefront function $U(\xi)$ has non-zero values only when ξ takes values of multiples integer of $1/S$. This behavior describes the existence of multiple diffractive orders.

3.1.1. Diffraction efficiency

Diffraction efficiency (η) of a hologram is defined as the ratio of the intensity values of the diffracted wavefront to the intensity of the incident wavefront,

$$\eta = \frac{|U(\xi)|^2}{|U_0(\xi)|^2} \tag{4}$$

Diffraction efficiency for all orders are computed by evaluating the intensity values at the particular diffraction orders using Eq. (3). Hence

$m = 0$

$$\eta|_{m=0} = A_0^2(1-D)^2 + A_1^2 D^2 + 2A_0 A_1 D(1-D)\cos(\phi) \tag{5}$$

$m = \pm 1, \pm 2, \ldots$

$$\eta|_{m\neq 0} = \left[A_0^2 + A_1^2 - 2A_0 A_1 \cos(\phi)\right] D^2 \sin c^2(mD) \tag{6}$$

3.1.2. Wavefront phase

Diffraction wavefront phase function can also be retrieved from Eq. (3). The diffraction wavefront phase function, Ψ, is determined as:

$$\tan(\Psi) = \frac{\mathrm{Im}\{U(\xi)\}}{\mathrm{Re}\{U(\xi)\}} \tag{7}$$

For different diffraction orders, the phase functions are:

$m = 0$

$$\tan(\Psi)_{m=0} = \frac{DA_1 \sin(\phi)}{A_0(1-D) + A_1 D \cos(\phi)} \tag{8}$$

$m = \pm 1, \pm 2, \ldots$

$$\tan(\Psi)_{m\neq 0} = \frac{A_1 \sin(\phi) \cdot \sin c(mD)}{[-A_0 + A_1 \cos(\phi)] \cdot \sin c(mD)} \tag{9}$$

The phase value can be obtained by taking the arctangent of these equations.

Notice that the sinc(mD) functions are left in both the numerator and denominator of Eq. (9); they are needed to preserve the sign information for the phase unwrapping process. The phase unwrapping process uses the sign information of the real and the imaginary parts of the complex wavefront, $U(\xi)$, to allow calculation of phase in a 0 to 2π period. The new phase values are then evaluated point by point. Any integer multiple of 2π can be added or subtracted from the phase value to force the phase function to be continuous.

3.1.3. Phase sensitivity to duty-cycle

We have shown that diffracted wavefront phase can be expressed as a function of duty-cycle and phase depth. By taking the first order derivative of Eqs. (8) and (9) with respect to either duty-cycle or phase depth, the phase deviations due to variations in duty-cycle or phase depth are determined. These deviations are defined as the "wavefront sensitivity functions". Eqs. (10) and (11) show the wavefront sensitivity functions that resulted from one unit variation in the grating duty-cycle.

$m = 0$:

$$\frac{\partial \Psi_{m=0}}{\partial D} = \frac{A_0 A_1 \sin\phi}{A_1^2 D^2 + A_0^2 (1-D)^2 + 2A_0 A_1 D(1-D)\cos\phi} \tag{10}$$

$m = \pm 1, \pm 2, \ldots$:

$$\frac{\partial \Psi_{m\neq 0}}{\partial D} = \begin{cases} \infty, & \text{for } \operatorname{sinc}(mD) = 0 \\ 0, & \text{otherwise} \end{cases} \tag{11}$$

Notice that duty-cycle errors produce wavefront phase errors only in the zero-order diffraction beam. Diffraction wavefront phase is not sensitive to CGH duty-cycle errors at non-zero diffraction orders.

3.1.4. Phase sensitivity to etch depth

Diffraction wavefront phase sensitivities to CGH etching depth variations at different diffraction orders are also determined from Eq. (8) and (9). Eq. (12) and (13) give the zero-order and the non-zero order wavefront sensitivity functions in terms of phase depth variations.

$m = 0$:

$$\begin{aligned} \frac{\partial \Psi_{m=0}}{\partial \phi} &= \frac{1}{1 + [\tan(\Psi)_{m=0}]^2} \cdot \frac{\partial \tan(\Psi)_{m=0}}{\partial \phi} \\ &= \frac{A_1^2 D^2 + A_0 A_1 D(1-D)\cos\phi}{A_1^2 D^2 + A_0^2 (1-D)^2 + 2A_0 A_1 D(1-D)\cos\phi} \end{aligned} \tag{12}$$

$m = \pm 1, \pm 2, \ldots$:

$$\begin{aligned} \frac{\partial \Psi_{m\neq 0}}{\partial \phi} &= \frac{1}{1 + [\tan(\Psi)_{m\neq 0}]^2} \cdot \frac{\partial \tan(\Psi)_{m\neq 0}}{\partial \phi} \\ &= \frac{A_1^2 - A_0 A_1 \cos\phi}{A_1^2 + A_0^2 - 2A_0 A_1 \cos\phi} \end{aligned} \tag{13}$$

The wavefront sensitivity functions (Eq. (10) through (13)) provide a means of calculating the phase changes in the wavefront that result from duty-cycle or phase depth variations. They can be used to identify hologram structures, which are

the most or the least sensitive to duty-cycle and phase depth fabrication uncertainties. The information may also be used to estimate error budgets for applications using CGHs.

3.1.5. Pattern Distortion

The displacement of the recorded fringe in a CGH from its ideal position is commonly referred to as pattern distortion. The amount of wavefront phase errors produced by the CGH pattern distortions can be expressed as a product of the gradient of the diffracted wavefront function and the pattern distortion vector $\vec{E}(x,y)$[5]:

$$\Delta W(x,y) = -\vec{\nabla} W_\lambda(x,y) \cdot \vec{E}(x,y) \tag{14}$$

where:

$\Delta W(x,y)$ = wavefront phase error;

$W_\lambda(x,y)$ = diffraction wavefront;

$\vec{\nabla} W_\lambda(x,y)$ = gradient of the diffraction wavefront (in the direction that is perpendicular to the fringes);

$\vec{E}(x,y)$ = CGH pattern distortion vector.

Therefore, for a linear grating, wavefront phase errors produced by grating pattern distortions in the m^{th} order beam can be calculated as:

$$\Delta W(x,y) = -m\lambda \frac{\varepsilon(x,y)}{S(x,y)} \tag{15}$$

where:

$\varepsilon(x,y)$ = grating position error in direction perpendicular to the fringes;
$S(x,y)$ = localized fringe spacing;

The produced wavefront phase errors due to pattern distortions are linearly proportional to the diffraction order number and inversely proportional to the local fringe spacing. Furthermore, CGH pattern distortion errors do not affect the zero-order diffracted beam.

3.2. CGH Substrate Errors

Typical CGH substrate errors are low spatial frequency surface figure errors that are responsible for the low spatial frequency wavefront aberrations in the diffracted wavefront. Fig. 2 gives a simple demonstration. For instance, in a reflection hologram setup, a surface defect on a CGH substrate with a peak-to-valley deviation of δs will produce a phase error in the reflected wavefront that equals $2\delta s$ because of the double path configuration. A transmission hologram that has the same peak-to-valley surface defect, on the other hand, will produce a wavefront phase error that is $(n-1)\delta s$, where n is the index of refraction of the substrate material.

One method of eliminating figure errors in a CGH is to measure the flatness of the substrate before the grating patterns are applied. This procedure is usually done using a Fizeau interferometer with a flat reference.

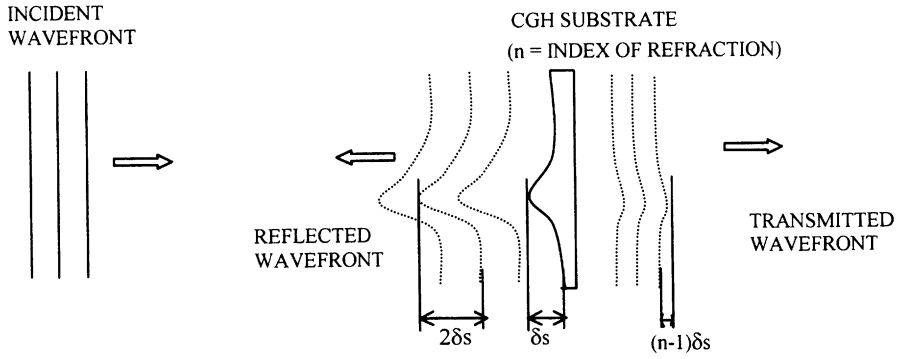

Fig. 2 Wavefront deviations due to substrate surface defects for both reflective and transmissive type holograms.

4. EXPERIMENTAL ANALYSIS

To validate the diffraction model, two custom holograms were fabricated: one is phase hologram and the other is chrome-on-glass hologram. The phase hologram was designed with duty-cycle and etching depths varied across hologram and the chrome-on-glass hologram was designed with only varied duty-cycle values. Both holograms were measured using phase-shifting interferometers. The results of phase sensitivity measurements for both holograms were compared with theoretical models. The experimental data agree with the theoretical analysis.[6] Fig. 3 illustrates an interferogram for the zero-order phase hologram.

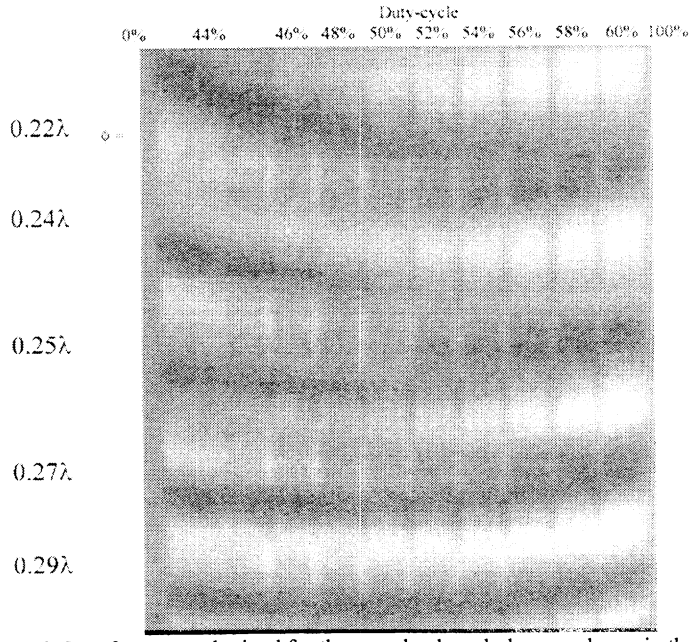

Fig. 3 Interferogram obtained for the sample phase hologram shown in the zero-order. (Note the phase shift around the center of the pattern).

5. ERRORS ANALYSIS OF A PHASE CGH

When applying CGHs in optical testing, it is necessary to evaluate the CGH in order to assure the validation and accuracy of the measured results. An example of a phase CGH incorporated with a Fizeau interferometer for testing aspheric optical components is shown in Fig. 4.

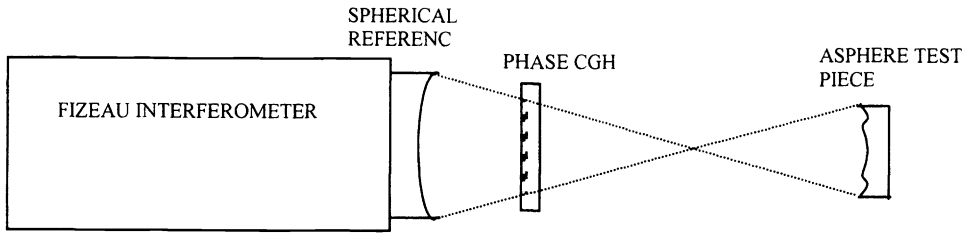

Fig. 4 Asphere metrology uses a Fizeau interferometer with a phase CGH.

In this example, typical values of phase CGH parameters are assigned. The example phase CGH is designed to be used in the 1st order transmission mode. The hologram is made by a glass substrate with an index of refraction of 1.5. It has a grating groove depth of π radians and a 50% duty-cycle. A potential pattern distortion of 1μm is assumed. The averaged fringe spacing on the CGH is approximately 40 um. The phase CGH has a RMS substrate figure error of $\lambda/10$ on both the front and the back surface.

To determine wavefront phase deviations caused by CGH fabrication errors, wavefront phase errors analysis results obtained in the previous section are employed. It should be obvious that surface figure errors from both the front and the back surface of the CGH contribute to aberrations in the diffracted wavefront, since the hologram is used in the transmission mode. The errors contributed by each surface is $\lambda/20$. The effect of pattern distortion to diffracted phase is proportional to the diffraction order number and inversely proportional to the grating spacing of $\lambda/40$ (Eq. 15). The first order wavefront phase deviations due to duty-cycle and grating groove depth errors are determined using wavefront sensitivity functions, Eqs (11) and (13). Duty-cycle deviations have no effects on the wavefront phase since the hologram is operated at its 1st diffraction order. A variation of five percent in phase depth would generate a $\lambda/80$ wavefront phase change. Since the test beam passes through the CGH twice in this setup, the total wavefront phase error for the setup is twice the value of the calculated error per pass. The calculated wavefront phase errors per pass for each error source are listed below:

Table 1 Diffraction wavefront phase errors from CGH fabrication uncertainties.

Source of Errors	Fabrication Tolerances	Wavefront Phase Errors per Pass
RMS Substrate Fig. Error (Front Surface)	$\lambda/10$	$\lambda/20$
RMS Substrate Fig. Error (Back Surface)	$\lambda/10$	$\lambda/20$
Pattern Distortion	±1 um	$\pm\lambda/40$
Grating Groove Depth Error	±5%	$\pm\lambda/80$
Duty-cycle Error	±2%	0
Root-Sum-Squared Errors :		$\pm 0.076\lambda$

Assuming the calculated CGH errors are un-correlated to each other, the total wavefront phase errors for the phase hologram can be estimated as the root-sum-square (RSS) of these errors. The calculation shows that the estimated diffracted wavefront phase errors produced by fabrication uncertainties and tolerance in the phase CGH is approximately 0.152λ including the effect of the double path of the test beam. In other words, the accuracy of the aspheric measurement

using the setup in Fig. 3 and the example CGH is limited by $\pm 0.152\lambda$ even when other sources of errors, such as interferometer errors and air turbulence, are eliminated.

As shown in Table 1, the largest individual error source is the substrate figure errors of the CGH. Normally the substrate error may be identified and eliminated. CGH substrate errors can be measured using the zero-order diffraction beam. In this example, however, the phase grating is constructed by a 50% duty-cycle and $\lambda/2$ phase depth. The zero-order diffracted wavefront phase has extremely high sensitivities to duty-cycle variations for a grating with a 50% duty-cycle and $\lambda/2$ phase depth (see Fig. 5). In other words, a 1% duty-cycle fabrication error on the grating could produce up to $\lambda/2$ wavefront phase deviations. This phase error overwhelms the effects of the CGH substrate error in the zero diffraction order and prohibits the substrate figure measurement in this example.

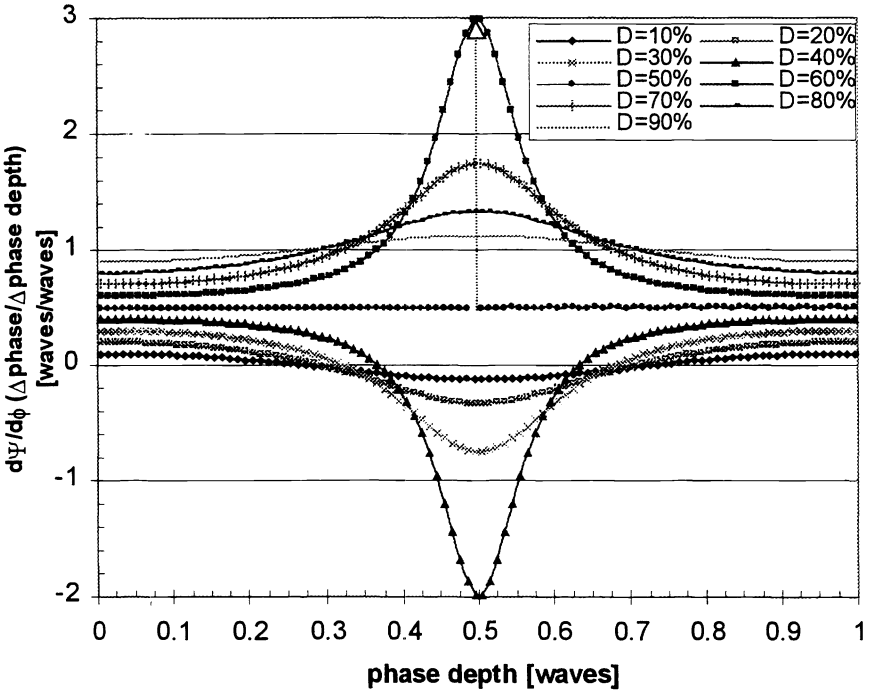

Fig. 5 Wavefront phase sensitivity of phase grating to grating phase depth variation for the zero-order beam for various duty-cycle values.

6. CONCLUSIONS

In this paper, we have studied CGH fabrication errors and their impacts on diffraction wavefronts. Theoretical modeling of CGHs with fringe duty-cycle and etch depth variations are presented. Analytical solutions are obtained and are summarized in the table below.

Table 2 Summary of equations for diffraction analysis.

	Zero order ($m = 0$)	**Non-zero order ($m \pm 1, \pm 2, \ldots$)**
η	$A_0^2(1-D)^2 + A_1^2 D^2 + 2A_0A_1D(1-D)\cos(\phi)$	$\left[A_0^2 + A_1^2 - 2A_0A_1\cos(\phi)\right]D^2\,\mathrm{sinc}^2(mD)$
$\tan(\Psi)$	$\dfrac{A_1 D\sin(\phi)}{A_0(1-D) + A_1 D\cos(\phi)}$	$\dfrac{A_1\sin(\phi)\cdot\mathrm{sinc}(mD)}{[-A_0 + A_1\cos(\phi)]\cdot\mathrm{sinc}(mD)}$
$\dfrac{d\Psi}{dD}$	$\dfrac{A_0A_1\sin\phi}{A_1^2D^2 + A_0^2(1-D)^2 + 2A_0A_1D(1-D)\cos\phi}$	$\begin{cases}\infty, & \text{for } \mathrm{sinc}(mD) = 0\\ 0, & \text{otherwise}\end{cases}$
$\dfrac{d\Psi}{d\phi}$	$\dfrac{A_1^2D^2 + A_0A_1D(1-D)\cos\phi}{A_1^2D^2 + A_0^2(1-D)^2 + 2A_0A_1D(1-D)\cos\phi}$	$\dfrac{A_1^2 - A_0A_1\cos\phi}{A_1^2 + A_0^2 - 2A_0A_1\cos\phi}$

The theoretical results are validated by experimental data. Applications of wavefront sensitivity functions in optical testing are demonstrated. The introduction of the wavefront sensitivity functions provides a quick and more intuitive method of CGH error analysis and error budgeting. The results of this research provide guidance to tolerance analysis of CGHs in the field of optical testing. They may also be used to direct CGH designs that will reduce or eliminate effects from fabrication errors.

ACKNOWLEDGMENTS

This work has been supported in part by the Eastman Kodak Company project number: 98Z900031461.

REFERENCES

[1]. Lohmann, A.W. and D. P. Paris, " Binary Fraunhofer holograms, generated by computer," Appl. Opt., 6, 1739-1748 (1967).

[2]. Burge, J. H. "Applications of computer-generated holograms for interferometric measurement of large aspheric optics," Proc. SPIE, **2576**, 258-269 (1995).

[3]. Goodman, J. W., *Introduction to Fourier Optics 2nd Ed.,* McGraw-Hill, Inc., N.Y., 1996.

[4]. Born, M. and E. Wolf, *Principles of Optics 6th Ed.,* Cambridge University Press, N.Y., 1980.

[5]. Fercher, A. F. "Computer-generated holograms for testing optical elements: error analysis and error compensation," Optica Acta, **23**, 347-365 (1976).

[6]. Chang, Y. C. "Diffraction wavefront analysis of computer-generated holograms," Ph.D. dissertation, Optical Sciences Center, University of Arizona, 1999.